#### Research Article

Yongzhi Zhang, Yipeng Wang\*, Hurong Duan, Yang Gao, and Jiashuang Jiao

## A non-uniform dip slip formula to calculate the coseismic deformation: Case study of Tohoku Mw9.0 Earthquake

https://doi.org/10.1515/geo-2019-0078 Received Mar 26, 2019; accepted Nov 05, 2019

**Abstract:** The distribution of slip faults along the fault plane plays a special role in the kinetic pattern of tectonic deformation. To better understand the coseismic deformation and geodynamics of the earthquake, this paper applied the pile-up theory and derived an analytical formula to describe the non-uniform slip distribution along the fault width. To validate the new formula, it was tested with the coseismic displacements at the global positioning system (GPS) stations for the Tohoku earthquake in 11 March, 2011. Then, the computed horizontal and vertical displacements calculated using NDSM were compared to back-slip model (BSM) using GPS data obtained from the Jet Propulsion Laboratory (JPL). Finally, the theoretical analysis revealed that the analytical formulas derived here can be perceived as the expansion and perfection of the uniform dislocation model. Meanwhile, our results showed that the characteristics of the spatial distribution deformation from NDSM are similar to those derived by GPS measurements. Furthermore, the near-field RMS errors indicated that the horizontal displacements estimated using NDSM is 27.5%, and 35.6% for the vertical components. Our new formulas and findings could assist better portray the crustal deformation in some region and geodynamics in specific earthquake.

**Keywords:** Pile-up theory, Non-uniform dip slip model(NDSM), Coseismic deformation, Back-slip model(BSM), Global positioning system(GPS)

Yongzhi Zhang, Hurong Duan, Yang Gao, Jiashuang Jiao: Chang'an University xi'an, China

#### 1 Introduction

Source models of earthquakes based on geodetic data provide invaluable insights about the earthquake rupture process. Since surface geodetic data are commonly interpreted using the uniform elastic dislocations embedded in the half-space [1-3], it can be referred to as the elastic dislocation models (EDMs). Heki et al., successfully applied an EDM to describe the fault slip [4]. The back-slip model [5], the simplest model among EDMs, is widely applied for modelling interseismic deformation (by incorporating geodetic data) in subduction zones [6–8]. Nonetheless, some previous studies, for example, Savage et al., [8] adopted a dislocation model to calculate the deformation in the rupture zone of the 1964 Alaska earthquake from 1993 to 1997. Whilst their measured deformation of the Prince William Sound geodetic array roughly matched the expected results of the back slip model (BSM) model in subduction zone [8], some trends could not be explained by this model (e.g., a zone of extension arcward of the downdip end of the locked zone). This might be because the application of the Okada-like uniform theory assumed that the fault resembled a rectangular plane with a uniform slip. Although the uniform slip assumption has the advantage of simplifying a study problem, it does not consistently represent the actual phenomenon. In a sense, the correlated results might contain inaccurate elements (i.e., supposing uniform slip of the fault would cause displacement and stress singularity on the boundary of the dislocation plane). Therefore, it is worthwhile to study the nonuniform slip of fault plane. However, there is no publication about the analytical formulas which describe the dip slip along the fault width. To address this shortfall, our earlier study performed an literature review and reported that the dislocation pile-up theory can effectively describe a series of crystal defects (slip bands, cracks, and twins); and gave a well constrained solution for elastic fields should a defect is locked at both ends [9]. More recently, a number of studies investigated the dislocation pile-up in crystals [10-12]. These models coincided with the experimental data,

<sup>\*</sup>Corresponding Author: Yipeng Wang: Chang'an University xi'an, China; Email: ypwchd@foxmail.com

and predicted the size of the yield stress. Based on the pile-up theory, we propose a non-uniform dip slip model (NDSM) which consists of a non-uniform dip-slip fault of finite width in an elastic half-space. According to this theory, the slip distribution parameters along the fault plane can be obtained and applied as a function of the fault's geometrical parameters. This model is especially useful when the geological setting of fault is double-ended pile-up by obstacles.

To study the phenomena of non-uniform slip fault, we firstly derive the expression of NDSM in accordance to the pile-up theory. Secondly, we incorporate the high-precision GPS data from Jet Propulsion Laboratory (JPL)(California,USA) into this formula to compute the deformation of Tohoku earthquake. Finally, we discuss the characteristics of the coseismic deformation predicted using the NDSM; and compare them to the horizontal and vertical deformation results calculated using the BSM Model.

## 2 Methodology

#### 2.1 The analytical formulas of NDSM

Figure 2 illustrates the theoretical model of a fault. In reality, every fault has its dominant direction. Hence, it is relevent to investigate the fault slip distribution in theory and application. The physical framework of pile-up theory can be simplified as follows: Suppose the crystalline dislocations under two shear stresses are piled up between two hampers. After adjustment and finally arriving at equilibrium, the discrete dislocation equation can be written as [13]:

$$\tau b + \frac{\mu b^2}{2\pi (1 - \nu)} \sum_{i=i+1} \frac{1}{y_i - y_i} = 0$$
 (1)

For a continuous distribution of the dislocation density on the dip slip plane of the fault, its equation is:

$$D\left(y'\right) = \frac{1}{b}\frac{db}{dy'}\tag{2}$$

The analytical formula of the non-uniform dip slip model can be derived as:

By setting the x-axis parallel to the strike component of the fault, the y-axis is normal to strike component and the z-axis is heading downward vertically. Here, L = length of the fault, W = width of the fault,  $\delta$  = dip angle, the colored arrows indicate the non-uniform dip slip distributions of the hanging wall relative to the foot wall. The dislocations influenced by the average shear on the dip slip

fault plane are piled-up at the lower and upper ends of the fault (Figure 2). After adjustment and eventual equilibrium state, the equation of dislocation groups for a homogeneous and isotropic elastic medium can be expressed as:

$$\tau b = \frac{\mu b^2}{2\pi (1 - \nu)} \int_{-W\cos\delta}^{W\cos\delta} \frac{D(y')}{y' - y} dy'$$
 (3)

where b is Burgers vector [14],  $\mu$  is Lame's constants of a medium,  $\nu$  is Poisson's ratio,  $\tau$  is the average shear stress. The equilibrium equation (3) can be rewritten as:

$$\frac{2(1-\nu)\tau}{\mu b} = \frac{1}{\pi} \int_{-W'}^{W'} \frac{D(y')}{y'-y} dy'$$
 (4)

where now  $W' = W \cos \delta$ .

$$\frac{2\tau(1-\nu)}{\mu b} = \frac{1}{\pi} \int_{-1}^{1} \frac{f(\eta')}{\eta' - \eta} d\eta' \tag{5}$$

Equation (5) is the Cauchy type of the singular integral equation. To solve equation (5), the Hilbert transform can be applied for the function of f(y), which can be written as:  $H_X[f(y)] = \frac{1}{\pi} \int_{-1}^{1} \frac{f(y)}{y-x} dy$ . The Hilbert transform of the Chebyshev first and second polynomials are,

$$\begin{cases} T_n(\cos\theta) = \cos n\theta \\ U_n(\cos\theta) = \sin(n+1)\theta/\sin\theta \end{cases}$$
 (6)

$$\begin{cases} H_{x} \left[ \frac{Tn(y)}{(1-y^{2})^{\frac{1}{2}}} \right] = U_{n-1}(x) \\ H_{x} \left[ (1-y^{2})^{\frac{1}{2}} U_{n-1}(y) \right] = T_{n}(x) \end{cases}$$
 (7)

In equation (7), when n=1 and  $U_0=1$ , then the left term of equation (5) can be converted to  $\frac{2(1-\nu)\tau}{\mu b}=\frac{2(1-\nu)\tau}{\mu b}U_0$  and by incorporating this part into the equation (7), the following equation can be derived:

$$H_{\eta}\left[\frac{T_1(\eta)}{1/2}\right] = U_0(\eta) \tag{8}$$

By comparing equations (8) and (5), we get:

$$f(\eta) = \frac{2(1-\nu)\tau}{\mu b} \frac{\eta}{(1-\eta^2)^{\frac{1}{2}}}$$
(9)

and,

$$f(\eta) = D(y) = \frac{2(1-\nu)\tau}{\mu b} \frac{y}{\sqrt{W'^2 - y^2}}$$
(10)

Equation (10) displays the dislocation density function along the dip slip component of the fault in the elastic

earth crust. The relationship between the slip and its density along the dip slip component of the fault can be established as:

$$\frac{dV}{dy} = -bD(y) \tag{11}$$

By integrating the two sides of equation (11), the following formula can be obtained:

$$V = \int -\frac{(1-\nu)\tau}{\mu} \cdot \frac{2y}{(W'-y^2)^{\frac{1}{2}}} dy$$

$$= \frac{(1-\nu)\tau}{\mu} \sqrt{(W\cos\delta)^2 - y^2}$$
(12)

Next, from equation (12), the strike slip expression along fault plane derived by Zhang *et al*. [15]. Thus, the square of the total slip on the fault plane was calculated as follows:

$$T^{2} = U^{2} + V^{2}$$

$$= A^{2}\tau_{c}^{2}(L^{2} - x^{2}) + A^{2}\tau_{d}^{2}[(W\cos\delta)^{2} - V^{2}]$$
(13)

Finally, equation (13) represents a total slip expression to compute the displacements on the Earth's surface.

### 3 Geological setting

The Tohoku earthquake occurred in the north-east sea area of Japan, a zone at the intersection of the Philippine, Eurasian, North American and Pacific plates. At the location of the earthquake, the Pacific plate moves roughly westward with respect to the North America plate, and begins its westward descent beneath Japan at the Japan Trench. Consequently, strong earthquakes frequently occurred in this zone.

It is generally accepted that after an earthquake, the rupture length and width of a fault, and the slip magnitude of the fault's hanging wall relative to the foot wall, are proportional to the magnitude of the earthquake. Therefore, those parameters can be determined by using inversion method and earth surface observational datasets (e.g., geodetic data). A geometrical model which was constructed to characterize the seismic activities in this area is presented in Figure 1 [16].

In Figure 1, the model describes the relative motion between the Japanese mainland and the Pacific plate, with the lower part of the Japanese mainland extruded by the Pacific plate at the speed of 8 cm/yr [17]. In the smooth area between the two plates, it is easy to identify a stable sliding area with non-seismic activity. Nevertheless, a local asperity area can also be detected in the non-smooth area. Crustal deformation often occurs in the asperity area,

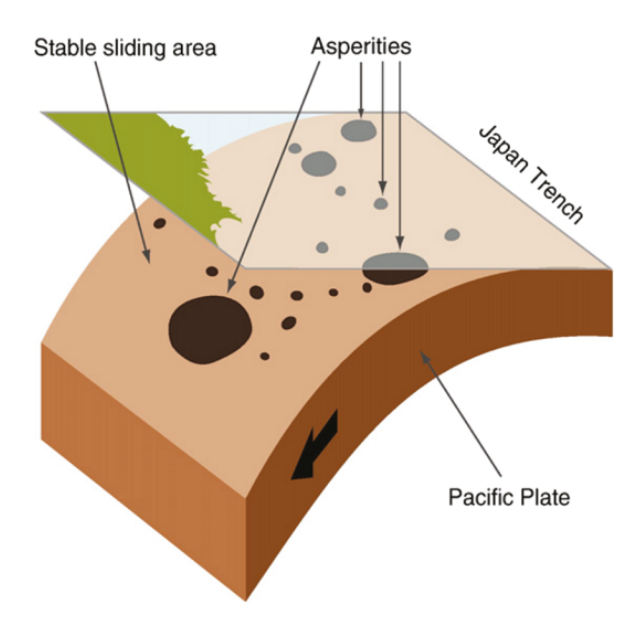


**Figure 1:** Schematic illustration of asperities and stable sliding given by Hasegawa *et al.* [16].

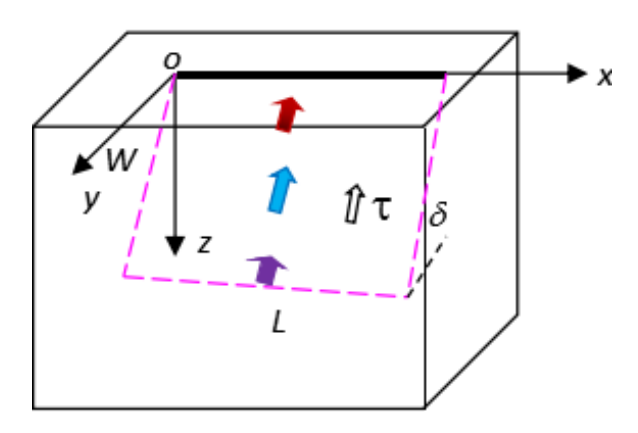


Figure 2: Geometrical fault model of non-uniform dip slip (x-axis is parallel to the strike component of the fault; y-axis is normal to the strike component and the z-axis is heading downward vertically and below the strike component; L is the length of the fault; W is the width of the fault,  $\delta$  is the dip angle of the fault plane;  $\tau$  is the average shear on the dip fault plane. Arrows represent the non-uniform slip of hanging wall relative to foot wall along the fault width)

with constant accumulation of elastic potential energy [18]. When the elastic potential energy hits the threshold value of the asperity system, an intense slip occurs within a short time. As a result, earthquakes with different magnitudes may happen in asperity areas [19]. To describe this coseismic deformation induced by the non-uniform dip slip between two plates, a non-uniform dip slip model of the hanging wall relative to the foot wall along a fault plane is built (see Figure 2).

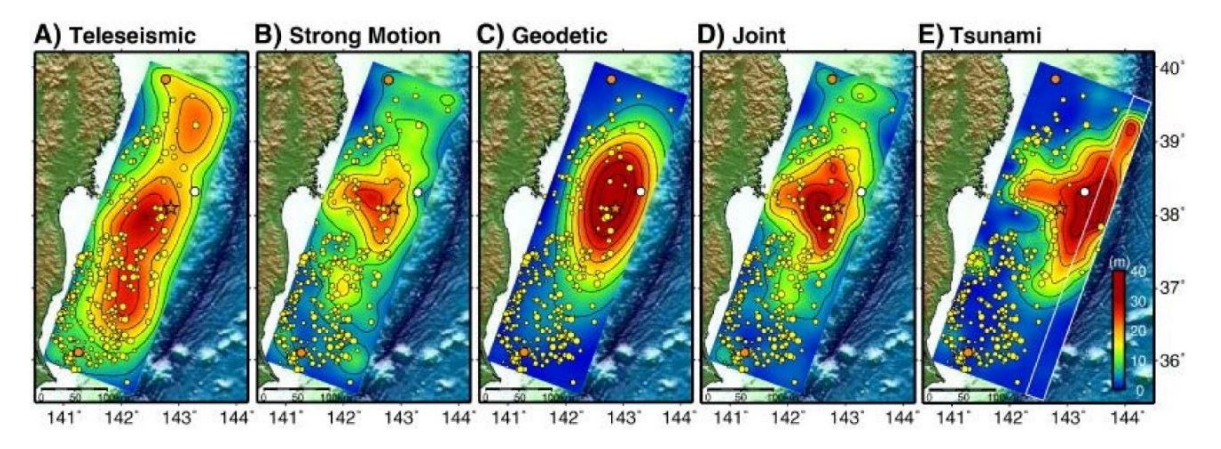


Figure 3: The slip distribution given by Koketsu et al. [29]

# 4 Application to GPS data for the 2011 Tohoku earthquake

#### 4.1 GPS data

GPS has been the most precise and convenient technology in geodetic surveying over the past two decades. Therefore, many studies (*e.g.*, Tiryakioglu *et al.*; Garrido *et al.*; Shestakov *et al.*) have applied global navigation satellite system (GNSS) technologies in 2011 Tohoku earthquake, and smoothly monitored its horizontal and vertical deformation [20–22].

In this article, we applied our new formula to the high precision GPS data (collected from JPL) for the 2011 Tohoku earthquake in order to validate the NDSM using the surface deformation (ftp://sideshow.jpl.nasa.gov/pub/usrs/ARIA/). A total of 1232 GPS sites in the seismic region (135-150°E,32-45°N) were calculated by the advanced rapid imaging and analysis (ARIA) team at JPL using the original data provided by the geospatial information authority (GSI) of Japan. Station positions and velocities were estimated in the International GNSS Service (IGS08) reference frame by using the QOCA software. Meanwhile, the data modeled by QOCA was performed using sequential kalman filtering (http://gipsy.jpl.nasa.gov/qoca/).

#### 4.2 Experiments

On March 11, 2011, a megathrust earthquake of Mw9.0 struck at the northeast sea area of Japan. According to the United States Geological Survey (USGS) report, the earthquake event occurred at the subduction zone plate boundary (38.297°N, 142.373°E) between the Pacific and North America plates with a depth of about 29.0 km.

It caused at least 15,703 people killed, 4,647 missing, 5,314 injured, the total economic loss in Japan was estimated at US\$309billion (https://earthquake.usgs.gov/ earthquakes/eventpage/official20110311054624120\_30/). Previous studies have applied different methods to investigate crustal deformation of Tohoku earthquake. Due to different data and methods, there are differences among the literatures about the source slip distribution of the Tohoku Mw9.0 earthquake [23–34]. The source model of the 2011 Tohoku earthquake was constructed from tsunami waveforms and crustal deformation data [35]. The seafloor displacements obtained from the tsunami simulations generated using uniform and non-uniform slip models have been evaluated [36]. In addition, Yokota et al. developed a unified source model for simulating the Tohoku earthquake through the joint inversion of teleseismic, strong motion, and geodetic datasets [37]. Wang et al. have simulated the slip distribution along the fault of the Tohoku earthquake from the joint inversion of GPS, InSAR and seafloor GPS/Acoustic measurements [38]. In addition, gravity data has been applied to construct a source model for the Tohoku earthquake [25]. Sun et al. and Nodai et al. interpreted the offshore movements of the 2011 Tohoku earthquake using the combined effect of after slip and viscoelastic stress relaxation [39, 40].

To understand the distribution characteristics of the slip along the earthquake fault plane (from the analytical NDSM model established in the above section), the surface horizontal displacements at GPS observations in the seismic region (135-150°E,32-45°N) were calculated using NDSM and compared to BSM results. The distribution of the slip on fault plane computed using NDSM was also compared to that obtained from the observed geodetic data (USGS, 2011) in this region. Figure 3 shows the distribution of source slip inversed from geodetic data. Figure 4 displays the source slip calculated from equation (12)

1018 — Y. Zhang et al. DE GRUYTER

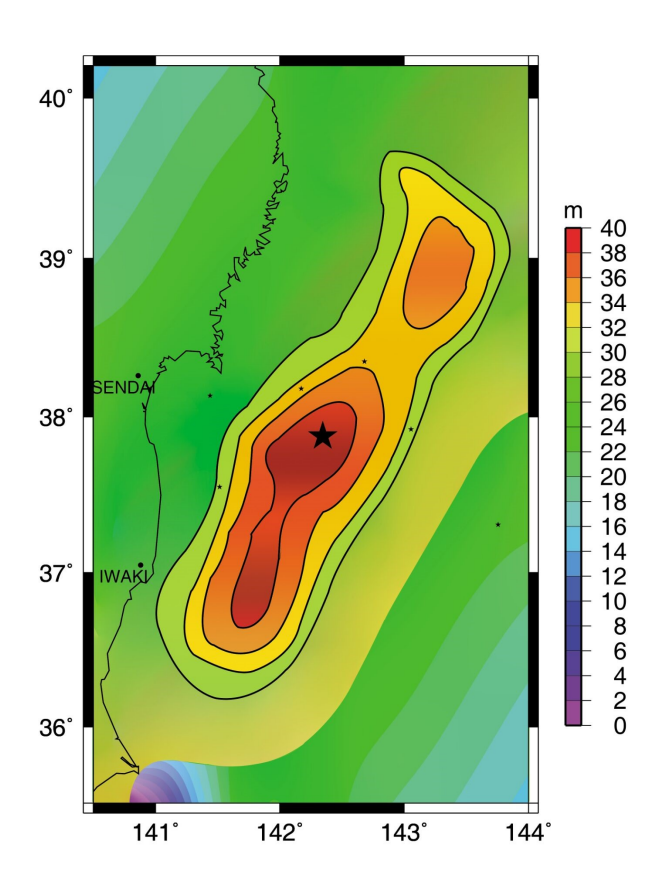


Figure 4: The slip distribution computed using NDSM

in this study. Comparing Figures 3 and [4], we note that the source slip conforms to an elliptical distribution pattern, with the semi-major axis located at about north-west  $45^{\circ}$  and the slip occurs somewhere between 0 and 40 meters.

According to the analytical NDSM, the procedures for computing the coseismic deformations are:

**(Step 1)** Apply the fault parameters in the designed earthquake fault model.

(Step 2) Divide the heterogeneous fault plane into 40×100 non-gap and non-overlap rectangular sub-faults with areas of 5km×5km. Inside each patch, the medium can be considered as elastic uniform. With respect to the whole fault plane, it is regarded as elastic non-uniform medium.rectangular sub-faults with areas of 5km×5km. Inside each patch,the medium can be considered as elastic uniform.With respect to the whole fault plane, it is regarded as elastic non-uniform medium.

The specific calculation approach is: On one hand, the dip slip along the fault width was computed using equation (12). On the other hand, the

**Table 1:** Parameters of fault in computation (BSM: parameters of back slip model; NDSM: parameters of non-uniform slip model, Geodetic: parameters of fault inversed from geodetic data; Tele: parameters of fault inversed from teleseismic data. Length, Width, Slip stand for the length, width and slip of the fault plane, respectively. DA is the dip angle of the fault, SA is the strike angle of the fault)

Fault	Length	Width	Slip	DA/°	SA/°
Models	/km	/km	/m		
BSM	500.0	200.0	0-40	3-15	45
NDSM	500.0	200.0	0-40	3-15	45
Geodetic	450.0	200.0	0-45	3-15	40
Tele	450	200.0	0-30	3-15	45

strike slip along the length was computed using the non-uniform strike slip formula [15], with the origin of coordinates located at the upper left corner of the fault. Finally, the total slip on the fault plane can be obtained using equation (13).

All seismogenic parameters used in this computation are shown in Table 1.

(Step 3) Calculate the displacements driven by slip on every sub-square fault from the BSM model. The final outcome of NDSM analysis is the sum of displacements computed on the 40×100 sub-square faults for each axis component (*i.e.*, east-west, north-south and up-down components). The initial values of the seismogenic fault parameters were adjusted using the try-and-error method, and subsequently used them for comparing to the values calculated using BSM and those recorded by GPS.

**(Step 4)** Finally, the displacements at different GPS locations computed using BSM and NDSM are presented in the diagram designed by the GMT software in Figure 5.

#### 4.3 Results

In Figure 5, blue arrows indicate the horizontal displacements calculated using NDSM, while black arrows represent the horizontal coseismic displacements derived by GPS at different GPS locations. The red stars designate the epicenters of the earthquake. By comparing the horizontal displacements calculated using the analytical NDSM to those observed by GPS recordings, we can see a high consistency in both magnitude and direction of surface displacements. To highlight the differences between NDSM and BSM, the horizontal displacements were also com-

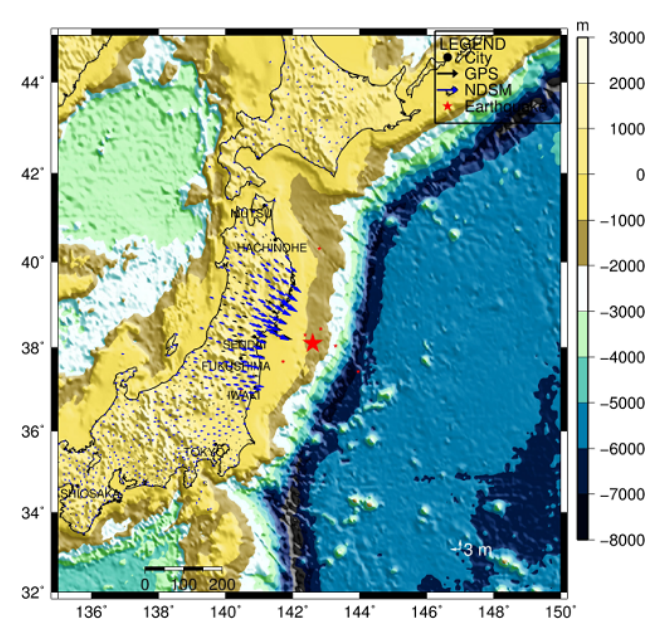


Figure 5: Comparison of horizontal displacements calculated using NDSM with those derived by GPS observations

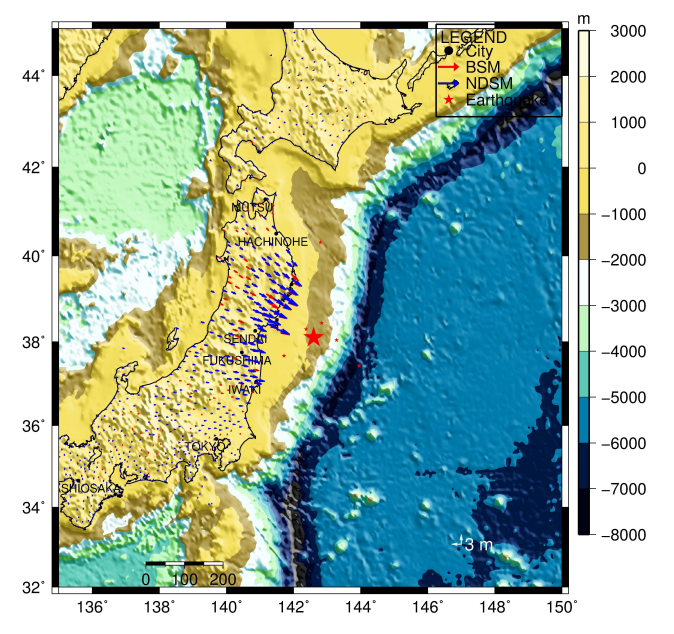


Figure 6: Comparison of horizontal displacements calculated using analytical NDSM and BSM (blue: displacements calculated using NDSM; red: displacements estimated using BSM)

puted at different GPS sites. Blue arrows indicate the horizontal displacements calculated using NDSM, and red arrows show those using BSM at the GPS sites. According to the results shown in Figure 6, a fine consistency can be observed between NDSM and BSM.

The deformation distribution caused by the earthquake appears more irregular in the vertical plane than in the horizontal one. Thus, it is difficult to obtain vertical

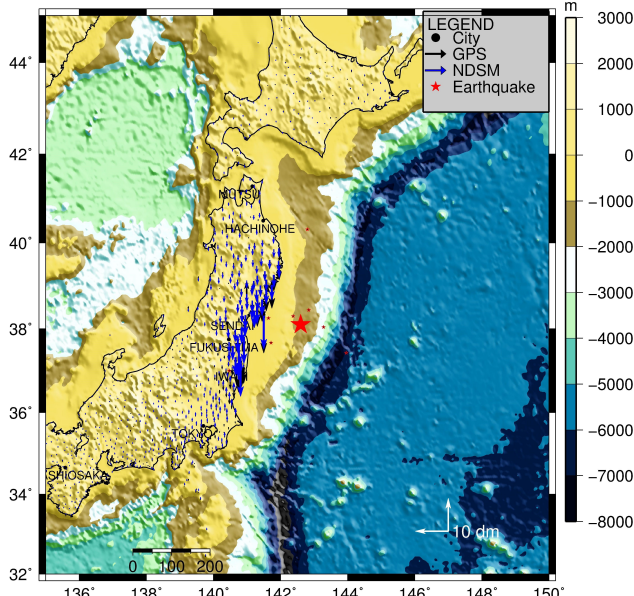


Figure 7: Comparison of vertical deformations estimated using NDSM and GPS recordings (blue: NDSM; black: GPS)

**Table 2:** Comparison of the RMS errors with the two computed displacements (BSM: back slip model; NDSM: non-uniform slip model; Difference: the ratio of NDSM to BSM)

Component	BSM/m	NDSM/m	Diffrence/%
Horiztonal	0.236	0.065	27.5
Vertical	0.129	0.046	35.6

displacements from the model. However, Figure 7 shows a good consistency between the vertical displacements calculated using this analytical formula and those observed by GPS in vertical direction.

## 5 Analysis

#### 5.1 RMS analysis

Whilst the above figures demonstrated that the results of BSM reflect the main trends of coseismic displacement, the NDSM with the dip slip of fault matches the observations relative to the ordinary uniform dislocation model. To examine the discrepancies between the BSM and NDSM more thoroughly, the root mean square (RMS) of the results differences between these two models and the observed ones are calculated using the following formula:

$$\hat{\sigma} = \sqrt{\sum_{i=1}^{N} |U_{obs}^{i} - U_{mod}^{i}|^{2} / N}$$
 (14)

	Dif(E-W:dm)	STD(dm)	Dif(S-N:dm)	STD(dm)	Dif(U-D:dm)	STD(dm)
Oka-Obs	0.137	1.070	0.068	0.672	0.088	0.430
NDSM-Obs	-0.009	0.892	0.105	0.657	0.083	0.380
NDSM-Oka	-0.138	0.606	-0.037	0.193	-0.005	0.070

Table 3: Differences among GPS, Okada model and NDSM in E-W, N-S and U-D directions

The RMS errors of the 50 GPS points are computed and displayed in Table 2. A comparison between the two models shows that the RMS gain for the horizontal displacement is 27.5%, while that for the vertical component is 35.6%. This reflects that the new method fits the observed displacements better than the BSM model. Hence, the new analytical formula which accounts for the non-uniform dip slip of fault is more reliable than that of the Okada-like uniform dislocation model.

To further explore the advantages of NDSM model, we compared the differences among GPS, Okada model and NDSM in E-W,N-S and U-D directions. Table 3 shows the statistical results of difference among displacements observed by GPS, Okada dislocation model and NDSM in East-West, North-South and Up-Down directions. In Table 3, the difference between displacements computed using Okada model minus those observed by GPS in East-West, North-South and Up-Down directions are calculated using statistic methods. The Dif column is the mean value of all displacement differences between Okada model and GPS measurement; DTD column is the standard deviation of the difference between displacements computed using Okada model minus those observed by GPS in the second row in Table 3. Similarly, the Dif column is the mean value of all displacement differences between NDSM and GPS measurement; and DTD column is the standard deviation of the difference between displacements computed using NDSM and those observed by GPS in the third row in Table 3. The Dif column is the mean value of all displacement differences between Okada model and NDSM; and DTD column is the standard deviation of the difference between displacements computed using Okada model and NDSM in the fourth row in Table 3.

The standard deviation between displacements computed using models and those by GPS measurements are the largest in E-W direction, but the smallest in Up-Down direction. The standard deviation of difference between NDSM and GPS measurements are smaller than those computed using Okada model and GPS measurements in East-West, North-South and Up-Down directions. The standard deviation of difference between NDSM and Okada model is smaller than that between models and GPS observations.

#### 5.2 Comparing to uniform-slip model

The displacement at random point d(y) on earth surface generates from point slip on fault plane is given by the equation:

$$d(y) = \int G(y, \zeta)m(\zeta)d\zeta \tag{15}$$

where d(y) is the displacement on earth's surface,  $G(y,\zeta)$  is Green function (*i.e.* kernal function) and  $m(\zeta)$  is the distribution function of slip. Since kernal function is often related to the physical characteristics of a specific medium, its expression can be derived analytically or using finite element method. The current Okada uniform dislocation formula is obtained under many conditions (including that the  $m(\zeta)$  in equation (15) is constant on the fault plane). To clarify the non-uniform analytical formula with the Okada rectangular dislocation model (where  $\delta=0$ ), we expand the equation (12) with Taylor series as follows:

$$V = \frac{\omega (1 - v) \tau}{\mu} \left[ 1 - \frac{1}{2!} \left( \frac{y}{\omega} \right)^2 - \frac{3}{4!} \left( \frac{y}{\omega} \right)^4 - \frac{45}{6!} \left( \frac{y}{\omega} \right)^6 + \cdots \right]$$
(16)

From equation (16) shows that the zero order term of non-uniform slip formula approximately equals the dislocation function model of Okada rectangular model. Hence, the new non-uniform expression in this paper can be perceived as the expansion and perfection of the uniform dislocation model.

#### 6 Discussion

The distribution of slip along a fault plane is the key to understand the physical process of an earthquake. However, the analytical formula that characterizes the distribution of slip along the width of the fault is rarely reported in previous studies. To explore this important challenge, we developed some non-uniform formulas to calculate the deformation on the earth surface. At first, we presented the mathematical background and then applied the new formulas to characterize the 2011 Tohoku earthquake.

We found that the co-seismic deformation calculated using NDSM is quite consistent with those estimated using BSM. The horizontal and vertical deformations (triggered by the Tohoku Mw9.0 earthquake) computed using NDSM have the similar space distribution characteristics with those derived by GPS observations. The standard deviation of the coseismic deformation difference between NSDM and GPS measurements are smaller than that between Okada model and GPS measurements. The standard deviation of difference between NDSM and Okada model is smaller than those between new models and GPS observations in East-West, North-South and Up-Down directions. Those differences might be due to faulty parameters, measurement error or the influence of aftershocks. The standard deviation of difference between displacements computed using NDSM and those observed by GPS are the largest in E-W direction and smallest in Up-Down direction.

#### 6.1 Different tectonic environments

Since the slip of fault caused by earthquakes takes place in the earth interior, the formula which expresses the distribution of dip slip along the fault width in accordance to the pile-up theory can be written as:

$$V = \frac{(1-\nu)\tau_d}{\mu} \sqrt{(W\cos\delta)^2 - y^2}$$

For the strike slip, the formula can be derived as:

$$U=\frac{(1-\nu)\tau_s}{u}\sqrt{L^2-x^2}.$$

The strike slip on the fault plane is unevenly distributed along the strike direction. At both ends of the fault, x = -L and x = L, the slip displacement on the fault surface is 0. At the middle of the fault, where x = 0, the displacement slip momentum of the fault is the largest.

#### 6.2 Moderate events

Current study provided a meaningful exploration about seismic fault study. However, the scope of this research was mainly limited to the dip-slip faults, and we adopted the new model for the Tohoku Mw9.0 earthquake in order to verify its utility. For moderate earthquakes (especially strike-slip and normal sense of slip) which are much less sampled that the Tohoku event, Avallone *et al.* applied very high rate GPS seismology data for moderatemagnitude earthquakes of the Mw 6.3 L'Aquila (central

Italy) event. They reported that GPS sampling rates greater than 2.5 Hz in the near field could be as useful as strong motion stations for earthquake source studies [41]. Melgar et al. obtained the model of fast rupture on a dipping strike-slip fault of the 2014 Mw6.1 Napa earthquake using real-time high-rate geodetic data. They highlighted the merit of combining GPS and strong motion data to produce seismogeodetic waveforms rather than relying GPS-only or seismic-only measurements of ground motion. They also confirmed that, with the existing real-time GPS and strong motion infrastructure, it is possible to determine the basic rupture features of the specific earthquake [42]. Chousianitis et al. inferred the slip model of the 2015 Mw6.5 Lefkada earthquake using teleseismic and seismic data combined with static and dynamic GPS displacements. Their joint inversion revealed a heterogeneous distribution pattern of rupture segmentation along the fault zone [43]. Cheloni et al. investigated the geodetic sequence model of the 2016 Central Italy Earthquake (Mw 6.1, 5.9, and 6.5, respectively). They used InSAR and GPS data to determine the source parameters of the main shocks [44]. Chousianitis et al. inferred the slip model of the 12 June 2017 Mw6.3 Lesvos earthquake using the static GPS displacement vectors and 1Hz GPS time series data. That study suggested that Coulomb stress calculations are dependable in such microplate boundaries [45]. In summary, we can deduce that the near-source data can be a prerequisite for the estimation which serves as a well-constrained source model for moderate events. As for NDSM model, it would be interesting to further explore the application of the near-field high-precision GPS data, waveforms, and etc. to constrain this new model.

#### 7 Conclusions

Traditionally, dislocation models are used to calculate the coseismic deformation due to movement of hanging wall relative to foot wall of the earthquake fault on the earth surface. However, the assumption of uniform fault slip can cause displacement and stress singularity on the boundary of the dislocation plane. In addition, this assumption cannot explain the phenomenon of extension arcward in the downdip end of the locked zone. There were no reports about analytic formula to characterize the dip slip along the fault width. Based on the dislocation pile-up theory developed for crystalline lattice behavior, we put forward an analytical formula. At first, the slip distribution along the fault of the Tohoku Mw9.0 earthquake was calculated using GPS data (collected from JPL) to evaluate the

validity and then improve the formula. Then, a comparison was performed. Finally, the following conclusions can be drawn:

When the lower and upper ends of the fault are fixed in the earth crust, the distribution function of the nonuniform dip slip displacements of the hanging wall relative to the foot wall along the fault width can be written as:

$$u = \frac{(1-\nu)\tau}{\mu} \sqrt{\left(W^2(\cos\delta)^2 - y^2\right)}$$

The slip distribution of the hanging wall relative to the foot wall, caused by the earthquake, has something to do with the length and width of the fault itself. The theoretical analysis using Taylor series revealed that formulas derived here approximately equals to the uniform Okada model (when in its zero order). In this sense, it can be viewed as the expansion and perfection of the uniform dislocation model.

- For the Tohoku Mw9.0 earthquake, the coseismic displacements computed using the analytical NDSM showed high consistency with those observed by GPS, both in magnitude and direction.
  - The results of NDSM revealed that the source slip of the Tohoku Mw9.0 earthquake conforms to an elliptical distribution pattern, with the semi-major axis located at about north-west 45° and the slip occurs somewhere between 0 and 40 meters. This might have explained the extension of the downdip end of this locked zone.
- RMS errors indicated that the coseismic deformation calculated using analytical NDSM is 27.5% for the horizontal displacement, and 35.6% for the vertical component (which are better than the BSM results).
- 3. Equation (13) illustrates that the total slip on rectangular fault plane with length L and width W, is of elliptical type, which gives slip as a function of y on a fault plane. By setting  $\delta = 0$  in equation (12), the result of the surface displacement is the same, as follows:  $b(s) = b_0 \sqrt{\left(1 \frac{s^2}{L^2}\right)}$  ( $0 \le s \le L$ ) [46], and

$$b(h) = b_0 \sqrt{\left(1 - \frac{h^2}{L^2}\right)} \ (0 \le h \le L) \ [47]$$
, which can be viewed as a particular case of our results.

Beside the limitation highlighted in the above section, the analytical formula of the NDSM gives satisfactory results and should support seismic characteristics assessment across different faults in future research.

**Acknowledgement:** We thank the ARIA team at JPL provided the preliminary high precision GPS data, and USGS

distributed the Seismic data. We thank editors and anonymous reviewers for their useful comments which led to an improvement of this manuscript.

This work is supported by the National Natural Science Foundation of China (nos:41374028, 41274083, 41304013). Some figures were generated by using the open-source software Generic Mapping Tools (GMT) [48].

**Competing Interests:** On behalf of all authors, the corresponding author states that there is no conflict of interest.

#### References

- Okada Y. Surface deformation due to shear and tensile faults in a half-space, Bulletin of the seismological society of America, 1985, 75(4): 1135-1154.
- [2] Okubo S. Gravity and potential changes due to shear and tensile faults in a half-space, Journal of Geophysical Research: Solid Earth, 1992, 97(B5): 7137-7144.
- [3] Koketsu K, Yokota Y, Nishimura N, et al. A unified source model for the 2011 Tohoku earthquake, Earth and Planetary Science Letters, 2011, 310(3-4): 480-487.
- [4] Heki K, Miyazaki S, Tsuji H. Silent fault slip following an interplate thrust earthquake at the Japan Trench, Nature, 1997, 386(6625): 595.
- [5] Savage J C. A dislocation model of strain accumulation and release at a subduction zone, Journal of Geophysical Research: Solid Earth, 1983, 88(B6): 4984-4996.
- [6] Khazaradze G, Klotz J. Short-and long-term effects of GPS measured crustal deformation rates along the south central Andes, Journal of Geophysical Research: Solid Earth, 2003, 108(B6).
- [7] Savage J C, Svarc J L. Postseismic deformation associated with the 1992 Mw= 7.3 Landers earthquake, southern California, Journal of Geophysical Research: Solid Earth, 1997, 102(B4): 7565-7577.
- [8] Savage J C, Svarc J L, Prescott W H, et al. Deformation across the rupture zone of the 1964 Alaska earthquake, 1993–1997, Journal of Geophysical Research: Solid Earth, 1998, 103(B9): 21275-21283.
- [9] Solovev V A, Zolotarev S N. The isotropic limit in anisotropic dislocation theory Green's functions in a crystal containing a dislocation pile-up, physica status solidi (b), 1979, 91(1): 319-323.
- [10] Liu D, He Y, Zhang B, et al. A continuum theory of stress gradient plasticity based on the dislocation pile-up model, Acta Materialia, 2014, 80: 350-364.
- [11] Kapp M W, Kirchlechner C, Pippan R, et al. Importance of dislocation pile-ups on the mechanical properties and the Bauschinger effect in microcantilevers, Journal of Materials Research, 2015, 30(6): 791-797.
- [12] Schmitt S, Schulz K, Dickel D, et al. Linking Micro-and Macro-scopic Aspects of a Dislocation Based Continuum Model by Investigating the Dislocation Double Pileup, PAMM, 2013, 13(1): 273-274.
- [13] Eshelby J D, Frank F C, Nabarro F R N. XLI. The equilibrium of linear arrays of dislocations, The London, Edinburgh, and Dublin

- Philosophical Magazine and Journal of Science, 1951, 42(327): 351-364.
- [14] Burgers J M. Physics. Some considerations on the fields of stress connected with dislocations in a regular crystal lattice, Selected Papers of JM Burgers. Springer, Dordrecht, 1995: 335-389.
- [15] Zhang Y Z. Zhao D J, Wang W D. Effects of Non-Uniform Strike Slip of Fault on Earth's Surface Deformation, Chinese Journal of Geophysics, 2009, 52(4): 865-871(in chinese).
- [16] Hasegawa A, Nakajima J, Uchida N, et al. Plate subduction, and generation of earthquakes and magmas in Japan as inferred from seismic observations: an overview, Gondwana Research, 2009, 16(3-4): 370-400.
- [17] DeMets C, Gordon R G, Argus D F, et al. Current plate motions, Geophysical journal international, 1990, 101(2): 425-478.
- [18] Lay T, Kanamori H. Earthquake doublets in the Solomon Islands, Physics of the Earth and Planetary Interiors, 1980, 21(4): 283-304
- [19] Hanks T C, Kanamori H. A moment magnitude scale, Journal of Geophysical Research: Solid Earth, 1979, 84(B5): 2348-2350.
- [20] Tiryakioglu I, Yigit C O, Yavasoglu H, et al. The determination of interseismic, coseismic and postseismic deformations caused by the Gökçeada-Samothraki earthquake (2014, Mw: 6.9) based on GNSS data, Journal of African Earth Sciences, 2017, 133: 86-94.
- [21] Garrido-Villén N, Berné-Valero J L, Antón-Merino A, et al. Displacement of GNSS permanent stations depending on the distance to the epicentre due to Japan's earthquake on 11 March 2011, Survey Review, 2013, 45(330): 159-165.
- [22] Shestakov N V, Takahashi H, Ohzono M, et al. Analysis of the far-field crustal displacements caused by the 2011 Great Tohoku earthquake inferred from continuous GPS observations, Tectonophysics, 2012, 524: 76-86.
- [23] Ammon C J, Lay T, Kanamori H, et al. A rupture model of the 2011 off the Pacific coast of Tohoku Earthquake, Earth, Planets and Space, 2011, 63(7): 33.
- [24] Wang C, Ding X, Shan X, et al. Slip distribution of the 2011 Tohoku earthquake derived from joint inversion of GPS, InSAR and seafloor GPS/acoustic measurements, Journal of Asian Earth Sciences, 2012, 57: 128-136.
- [25] Cambiotti G, Sabadini R. A source model for the great 2011 Tohoku earthquake (Mw= 9.1) from inversion of GRACE gravity data, Earth and Planetary Science Letters, 2012, 335: 72-79.
- [26] Garrido-Villén N, Berné-Valero J L, Antón-Merino A, et al. Displacement of GNSS permanent stations depending on the distance to the epicentre due to Japan's earthquake on 11 March 2011, Survey Review, 2013, 45(330): 159-165.
- [27] Kapp M W, Kirchlechner C, Pippan R, et al. Importance of dislocation pile-ups on the mechanical properties and the Bauschinger effect in microcantilevers, Journal of Materials Research, 2015, 30(6): 791-797.
- [28] Fukutani Y, Suppasri A, Imamura F. Stochastic analysis and uncertainty assessment of tsunami wave height using a random source parameter model that targets a Tohoku-type earthquake fault, Stochastic Environmental Research and Risk Assessment, 2015, 29(7): 1763-1779.
- [29] Koketsu K, Yokota Y, Nishimura N, et al. A unified source model for the 2011 Tohoku earthquake, Earth and Planetary Science Letters, 2011, 310(3-4): 480-487.
- [30] Kubo H, Kakehi Y. Source process of the 2011 Tohoku earthquake estimated from the joint inversion of teleseismic body waves and geodetic data including seafloor observation data: source model

- with enhanced reliability by using objectively determined inversion settings, Bulletin of the Seismological Society of America, 2013, 103(2B): 1195-1220.
- [31] Iinuma T, Hino R, Kido M, et al. Coseismic slip distribution of the 2011 off the Pacific Coast of Tohoku Earthquake (M9. 0) refined by means of seafloor geodetic data, Journal of Geophysical Research: Solid Earth, 2012, 117(B7):1236-1257.
- [32] Oishi Y, Imamura F, Sugawara D. Near-field tsunami inundation forecast using the parallel TUNAMI-N2 model: Application to the 2011 Tohoku-Oki earthquake combined with source inversions, Geophysical Research Letters, 2015, 42(4): 1083-1091.
- [33] Ozawa S, Nishimura T, Suito H, *et al*. Coseismic and postseismic slip of the 2011 magnitude-9 Tohoku-Oki earthquake, Nature, 2011, 475(7356): 373.
- [34] Wang W, Sun W, Wu Y, et al. Modification of fault slip models of the Mw 9.0 Tohoku Earthquake by far field GPS observations, Journal of Geodynamics, 2014, 75: 22-33(in chinese).
- [35] Hossen M J, Cummins P R, Dettmer J, et al. Tsunami waveform inversion for sea surface displacement following the 2011 Tohoku earthquake: Importance of dispersion and source kinematics, Journal of Geophysical Research: Solid Earth, 2015, 120(9): 6452-6473.
- [36] Ulutas E. Comparison of the seafloor displacement from uniform and non-uniform slip models on tsunami simulation of the 2011 Tohoku-Oki earthquake, Journal of Asian Earth Sciences, 2013, 62: 568-585.
- [37] Yokota Y, Koketsu K, Fujii Y, et al. Joint inversion of strong motion, teleseismic, geodetic, and tsunami datasets for the rupture process of the 2011 Tohoku earthquake, Geophysical Research Letters, 2011, 38(7):0028.
- [38] Wang C, Ding X, Shan X, et al. Slip distribution of the 2011 Tohoku earthquake derived from joint inversion of GPS, InSAR and seafloor GPS/acoustic measurements, Journal of Asian Earth Sciences, 2012, 57: 128-136.
- [39] Sun T, Wang K, linuma T, et al. Prevalence of viscoelastic relaxation after the 2011 Tohoku-oki earthquake, Nature, 2014, 514(7520): 84.
- [40] Noda A, Takahama T, Kawasato T, et al. Interpretation of offshore crustal movements following the 2011 Tohoku-oki earthquake by the combined effect of afterslip and viscoelastic stress relaxation, Pure and Applied Geophysics, 2018, 175(2): 559-572.
- [41] Avallone A, Marzario M, Cirella A, et al. Very high rate (10 Hz) GPS seismology for moderate-magnitude earthquakes: The case of the Mw 6.3 L'Aquila (central Italy) even, Journal of Geophysical Research: Solid Earth, 2011, 116(B2).
- [42] Melgar D, Geng J, Crowell B W, et al. Seismogeodesy of the 2014 Mw6. 1 Napa earthquake, California: Rapid response and modeling of fast rupture on a dipping strike-slip fault[J]. Journal of Geophysical Research: Solid Earth, 2015, 120(7): 5013-5033.
- [43] Chousianitis K, Konca A O, Tselentis G A, *et al.* Slip model of the 17 November 2015 Mw= 6.5 Lefkada earthquake from the joint inversion of geodetic and seismic data, Geophysical Research Letters, 2016, 43(15): 7973-7981.
- [44] Cheloni D, De Novellis V, Albano M, et al. Geodetic model of the 2016 Central Italy earthquake sequence inferred from InSAR and GPS data, Geophysical Research Letters, 2017, 44(13): 6778-6787
- [45] Chousianitis K, Konca A O. Coseismic slip distribution of the 12 June 2017 Mw= 6.3 Lesvos earthquake and imparted static stress changes to the neighboring crust, Journal of Geophysical

- Research: Solid Earth, 2018, 123(10): 8926-8936.
- [46] Godara Y, Sahrawat R K, Singh M. Static elastic deformation in an orthotropic half-space with rigid boundary model due to non-uniform long strike slip fault, Journal of Earth System Science, 2017, 126(7): 97.
- [47] Singh S J, Punia M, Rani S. Crustal deformation due to nonuniform slip along a long fault, Geophysical Journal International, 1994, 118(2): 411-427.
- [48] Wessel, P., Smith, W. H. F. New, improved version of Generic Mapping Tools released. Eos, Transactions American Geophysical Union, 1998, 79(47), 579.